JOURNAL OF MATERIALS SCIENCE 25 (1990) 1069–1075

Morphology and deposition rates of TiB_2 prepared by chemical vapour deposition of $TiCl_4 + B_2H_6$ system

MASAKAZU MUKAIDA, TAKASHI GOTO, TOSHIO HIRAI
Institute for Materials Research, Tohoku University, Sendai 980, Japan

Titanium diboride (TiB_2) deposits were obtained on a graphite substrate by chemical vapour deposition using $TiCl_4$, B_2H_6 and H_2 at deposition temperatures (T_{dep}) of 1323 to 1773 K and total gas pressures (P_{tot}) of 4 to 40 kPa. B/Ti molar ratio in the source gases [$2B_2H_6/TiCl_4$ ($m_{B/Ti}$)] was varied from 0.6 to 4. TiB_2 plates were prepared at $m_{B/Ti}$ = 0.6 to 2. The deposition rate increased with increasing T_{dep}. The largest value of the deposition rate was 1.4×10^{-7} m sec^{-1} (0.5 mm h^{-1}) at T_{dep} = 1773 K, P_{tot} = 40 kPa and $m_{B/Ti}$ = 0.6. The activation energies for the formation of CVD–TiB_2 plate were 41 to 51 kJ mol^{-1}. These values suggest that the diffusion of gaseous species through the boundary layer is a rate-determining process.

1. Introduction

Titanium diboride (TiB_2) is a promising new material in applications to cutting tools [1], letdown valves for coal conversion reactors [2] and the cathode of aluminium smelting cells [3] due to its superior wear and corrosion resistance [4]. TiB_2 is also a possible first-wall material for a fusion reactor due to its low atomic number (low-z) [5].

TiB_2 films have been prepared by sputtering [6] and chemical vapour deposition (CVD) [7], but the CVD techniques are known to be the most effective in preparing highly dense and pure TiB_2 films. In past studies, CVD–TiB_2 was prepared mainly by using $TiCl_4$ and BCl_3 as source gases [1, 8–17]. The largest reported deposition rate was 8.3×10^{-8} m sec^{-1} (0.3 mm h^{-1}) [8]. B_2H_6 gas has also been used as a boron source, and the deposition rates for the $TiCl_4 + B_2H_6$ system were generally higher than those for the $TiCl_4 + BCl_3$ system at temperatures below T_{dep} = 1073 K [18]. However, in the previous work, the CVD–TiB_2 prepared by the $TiCl_4 + B_2H_6$ system above T_{dep} = 1173 K were powdery [18]. High-quality CVD–TiB_2 films or plates have not been obtained using the $TiCl_4 + B_2H_6$ system above T_{dep} = 1173 K.

The present study aims to prepare high-quality TiB_2 plates at the highest possible deposition rate using the CVD of the $TiCl_4 + B_2H_6$ system at higher T_{dep}. In particular, this paper describes the effects of deposition conditions on the morphology and deposition rates of CVD–TiB_2. The difference in the formation mechanism for the CVD–TiB_2 between the $TiCl_4 + B_2H_6$ system and the $TiCl_4 + BCl_3$ system is also discussed.

2. Experimental procedure

The schematic diagram of the CVD apparatus is shown in Fig. 1. The graphite substrate (40 × 12 × 2 mm) was heated by transmitting an electric current. Liquid $TiCl_4$, B_2H_6 (5 vol %) + H_2 (95 vol %) mixture gas and H_2 gas were used as source materials. The total gas flow rate of H_2 was kept constant at 2.0×10^{-5} m^3 sec^{-1}, and the B/Ti molar ratio in the source gases ($m_{B/Ti}$) was controlled in the range of 0.6 to 4. The deposition temperatures (T_{dep}) ranged from 1323 to 1773 K, and the total gas pressures (P_{tot}) were varied from 4 to 40 kPa. The deposition time was 7.2 ksec. The deposition conditions are summarized in Table I.

The microstructure of the deposits was observed by scanning electron microscope (SEM) (Akashi: ALPHA-30W). The crystal structure of the deposits was examined by X-ray diffractometer (Rigaku: RAD-IIB, Ni filtered, CuKα). The thickness of the deposits was determined by an optical microscope. The deposition rate of the CVD–TiB_2 plates was calculated by the ratio x/t (x; thickness, t; time) since the thickness increased linearly with time. The density of all CVD–TiB_2 plates was constant (100% of theoretical density: 4.49×10^3 kg m^{-3}).

3. Results and discussion

3.1. Morphology

X-ray diffraction analysis indicated that all of the deposits obtained under varied deposition conditions were hexagonal type TiB_2. Typical surface and cross-sectional structures revealed by SEM for CVD–TiB_2

TABLE I Deposition conditions

Deposition temperature	1323–1773 K
Total gas pressure	4–40 kPa
Gas flow rate	
$TiCl_4$	2.2×10^{-7}–5.6×10^{-7} m^3 sec^{-1}
B_2H_6	1.7×10^{-7}–4.4×10^{-7} m^3 sec^{-1}
H_2	2.0×10^{-5} m^3 sec^{-1}
$2B_2H_6/TiCl_4$ ($m_{B/Ti}$)	0.6, 2, 4
Deposition time	7.2 ksec

0022–2461/90 $03.00 + .12

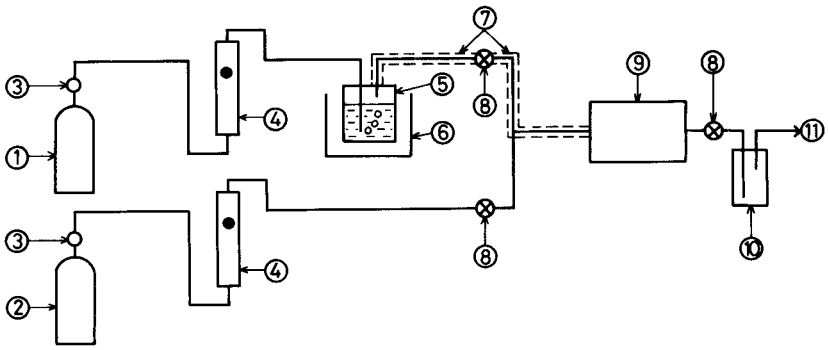

Figure 1 Schematic diagram of CVD apparatus. (1) H_2 gas, (2) B_2H_6 + H_2 gas, (3) pressure regulator, (4) flow meter, (5) $TiCl_4$ reservoir, (6) constant temperature bath, (7) ribbon heater, (8) valve, (9) reaction chamber, (10) cold trap, (11) rotary pump.

obtained in this experiment are shown in Figs 2 to 5. Fig. 2 shows the deposit prepared at T_{dep} = 1323 K, P_{tot} = 4 kPa and $m_{B/Ti}$ = 0.6. Both surface and cross-section are dense, homogeneous and plate-like. The granular TiB_2 shown in Fig. 3 was prepared at T_{dep} = 1373 K, P_{tot} = 13.3 kPa and $m_{B/Ti}$ = 4. The sizes of the granules were 0.2 to 0.5 mm in diameter. Fig. 4 shows the CVD–TiB_2 deposits prepared at T_{dep} = 1573 K, P_{tot} = 4 kPa and $m_{B/Ti}$ = 4. A long dendritic structure grew in the direction along the deposit growth. The columnar deposits of CVD–TiB_2 were obtained at T_{dep} = 1673 K, P_{tot} = 40 kPa and $m_{B/Ti}$ = 4 as shown in Fig. 5. Many faceted separate columns were observed. These crystals were elongated in the growth direction.

The relationship between the morphology and deposition conditions is summarized in Fig. 6. The CVD conditions to obtain the TiB_2 plates were $m_{B/Ti}$ = 0.6 at all T_{dep} and P_{tot}, while at $m_{B/Ti}$ = 2 CVD conditions were in the range of T_{dep} = 1573 to 1673 K at all P_{tot}.

The morphology of the CVD–TiB_2 plates can be divided into two groups. The first is a pebble structure and the second is a facet structure. The broken lines in Figs 6a and b indicate the boundary between the pebble and facet structure. When $m_{B/Ti}$ = 2, granular CVD–TiB_2 was obtained in the range of T_{dep} = 1573 to 1773 K. When $m_{B/Ti}$ = 4, no CVD–TiB_2 plate was obtained under any conditions. The structures varied from granule to dendrite to column with increasing T_{dep} and P_{tot}.

Fig. 7 shows the effect of the T_{dep} on the surface structure of CVD–TiB_2 plates at P_{tot} = 40 kPa and $m_{B/Ti}$ = 0.6. A smooth pebble structure was obtained below 1573 K, and the crystal facets appeared above 1673 K. The size of each facet increased with an increase in T_{dep}.

Fig. 8 shows the calculated CVD phase diagram at P_{tot} = 4 kPa. The solid and broken lines in Fig. 8 indicate the boundaries between TiB_2 and TiB_2 + B regions for the $TiCl_4$ + B_2H_6 (solid line) and the $TiCl_4$ + BCl_3 (broken line) systems. The SOLGASMIX-PV [19] was used for the thermodynamic calculations. Twenty-four gaseous species and five condensed phases of ⟨Ti⟩, ⟨B⟩, ⟨TiB⟩, ⟨TiB_2⟩ and ⟨TiH_2⟩ were considered in the calculation [20, 21]. For the $TiCl_4$ + B_2H_6 system, only the TiB_2 phase is expected to form deposits below $m_{B/Ti}$ of about 1.25 and a codeposit of free-B and TiB_2 are predicted at $m_{B/Ti}$ about 1.25. TiB_2 in single phase will be deposited even at higher $m_{B/Ti}$ when T_{dep} is low in both $TiCl_4$ + BCl_3 and $TiCl_4$ + B_2H_6 systems. In comparison, the $TiCl_4$ + BCl_3 system yields single phase TiB_2 in a much wider region of T_{dep} and $m_{B/Ti}$.

In the present work, even at $m_{B/Ti}$ = 4, free-B was not identified in the deposited CVD–TiB_2 by X-ray or chemical analyses. However, a large amount of boron and boron oxide powders were identified inside of the CVD chamber at $m_{B/Ti}$ = 4. It is supposed that the boron oxide powder is formed by the oxidation of the boron powder when the CVD chamber is exposed to air. The absence of free-B in the deposited CVD–TiB_2 at $m_{B/Ti}$ = 4 observed earlier may be due to the formation of free-B by homogeneous nucleation in gas phase.

Besmann and Spear [4] prepared CVD–TiB_2 using the $TiCl_4$ + BCl_3 system and reported that the resulting CVD–TiB_2 was plate-like at $m_{B/Ti}$ = 0.5 and

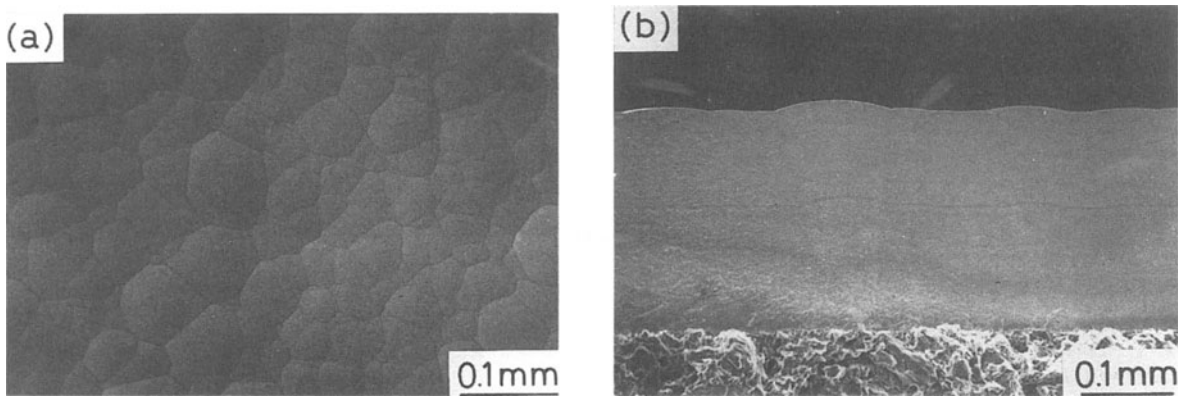

Figure 2 Scanning electron micrographs of the surface (a) and cross-section (b) of CVD–TiB_2 plate prepared at T_{dep} = 1323 K, P_{tot} = 4 kPa and $m_{B/Ti}$ = 0.6.

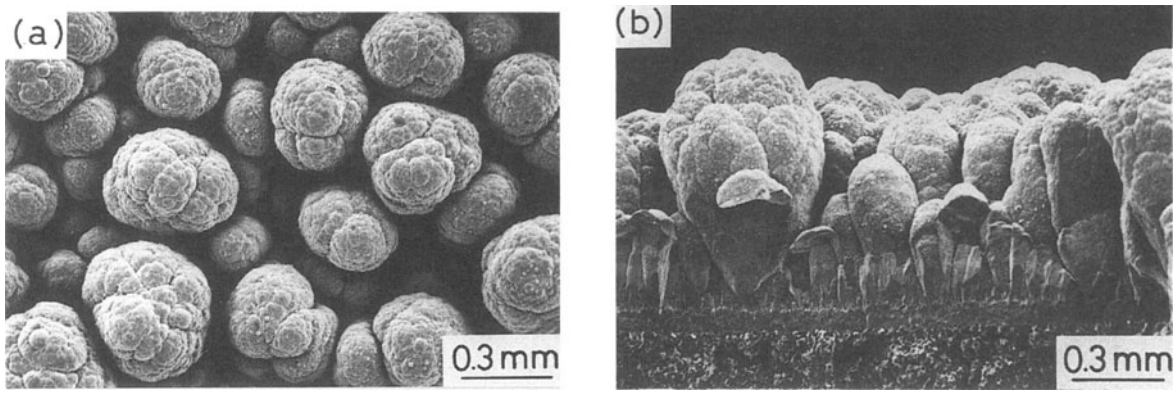

Figure 3 Scanning electron micrographs of the surface (a) and cross-section (b) of granular CVD–TiB_2 prepared at T_{dep} = 1373 K, P_{tot} = 13.3 kPa and $m_{B/Ti}$ = 4.

dendritic at $m_{B/Ti}$ = 4 to 8. They pointed out that dendritic CVD–TiB_2 formed at the conditions under which the codeposition of TiB_2 and free-B were predicted from thermodynamic calculations. The free-B particles formed in the gas phase by homogeneous nucleation may fall down onto the deposition surface. This tendency may have inhibited the formation of plate-like deposits and thus led to the formation of dendritic CVD–TiB_2.

Table II summarizes the deposition conditions and morphology of CVD–TiB_2. Many studies using the $TiCl_4$ + BCl_3 system reported that plate-like deposits were prepared below $m_{B/Ti}$ = 4 at all T_{dep} and the structure of deposits prepared over $m_{B/Ti}$ = 4 was porous or dendritic. This result may be caused by the formation of free-B particles in the gas phase as mentioned earlier. Takahashi and Kamiya [11] suggested that deposits contain amorphous free-B because the deposits were partially corroded by nitric acid, but the exact amount of free-B was not reported. Gebhardt and Cree [8] estimated from the low density of resulting CVD–TiB_2 deposit obtained at $m_{B/Ti}$ of about 3 that the amounts of free-B were 10 to 50 wt %, however, the quantitative chemical analysis was not presented.

Pierson and Mullendore [18] prepared CVD–TiB_2 using the $TiCl_4$ + B_2H_6 system. They reported that the CVD–TiB_2 films contained 15 wt % of free-B at $m_{B/Ti}$ = 2 and T_{dep} = 773 to 873 K, while the stoichiometric CVD–TiB_2 films were prepared at T_{dep} = 873 to 1223 K. However, the CVD–TiB_2 films also contained 0.5 to 3 wt % of Cl and the amount of Cl decreased with an increase in T_{dep}. The deposits were powdery over T_{dep} = 1223 K due to the homogeneous nucleation in the gas phase.

In the present work, plate-like CVD–TiB_2 were prepared even at higher T_{dep} of over 1323 K using the $TiCl_4$ + B_2H_6 system. It is considered that the direct heating of the substrate by electric current and the concentrated rapid gas flow around the substrate by the gas inlet nozzle must have prevented the occurrence of homogeneous nucleation of the free-B particles in the gas phase. Chemical analysis showed the absence of both free-B and Cl in the CVD–TiB_2 plates prepared in the present work. All of the deposits had stoichiometric composition.

3.2. Deposition rate

Fig. 9 shows the effect of T_{dep} on the deposition rate of CVD–TiB_2 plates at $m_{B/Ti}$ = 0.6. The deposition rate increased with an increase in T_{dep} at all P_{tot}. Below T_{dep} = 1473 K, the deposition rate was almost independent of P_{tot}, whereas, above T_{dep} = 1573 K the deposition rate increased with an increase in P_{tot}. The largest deposition rate of the CVD–TiB_2 plate in the present work was 1.4 × 10^{-7} m sec^{-1} (0.5 mm h^{-1}) at T_{dep} = 1773 K, P_{tot} = 40 kPa and $m_{B/Ti}$ = 0.6.

Fig. 10 summarizes the deposition rates of CVD–TiB_2 reported thus far. The present results are indicated in Fig. 10 by the shaded region. The value of

TABLE II Deposition conditions and morphology of CVD–TiB_2

System	Deposition conditions			Deposit	Morphology	Ref.
	T_{dep} (K)	P_{tot} (kPa)	$m_{B/Ti}$			
$TiCl_4$ + BCl_3	873–1373	–	0.1–4	TiB_2(+B)	plate	11
			10	TiB_2(+B)	porous	11
$TiCl_4$ + BCl_3	1173–1873	5.33–101.3	0.5	TiB_2	plate	1
			4–8	TiB_2	porous	1
$TiCl_4$ + BCl_3	1473–2073	1.33	3.23	TiB_2	plate	7
$TiCl_4$ + BCl_3	1473–1688	0.53–2.08	0.6	TiB_2	plate	8
			3.23	TiB_2(+B)	plate	8
			10.0	TiB_2(+B)	porous	8
$TiCl_4$ + B_2H_6	773–873	–	2	TiB_2 + B	plate	18
	873–1223			TiB_2	plate	18
$TiCl_4$ + B_2H_6	1323–1773	4–40	0.6–2	TiB_2	plate	present work
			4	TiB_2	porous	present work

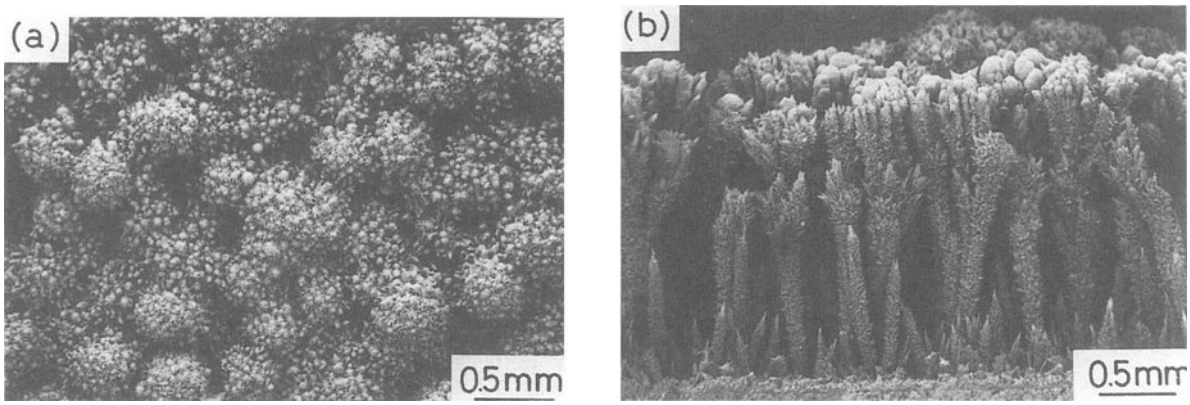

Figure 4 Scanning electron micrographs of the surface (a) and cross-section (b) of dendritic CVD-TiB_2 prepared at T_{dep} = 1573 K, P_{tot} = 4 kPa and $m_{B/Ti}$ = 4.

8.3×10^{-8} m sec^{-1} (0.3 mm h^{-1}) reported for the $TiCl_4 + BCl_3$ system [8] was the largest in the previous studies. Fig. 10 indicates that the present results are among the largest reported so far. CVD-TiB_2 has never been prepared below T_{dep} = 1000 K in the $TiCl_4 + BCl_3$ system, however, it is possible to prepare CVD-TiB_2 even at T_{dep} as low as 873 K in the $TiCl_4 + B_2H_6$ system. The deposition rates of CVD-TiB_2 in the $TiCl_4 + B_2H_6$ system tend to be higher than those in the $TiCl_4 + BCl_3$ system.

Fig. 11 shows a comparison of the theoretical deposition efficiency for CVD-TiB_2 between the $TiCl_4 + B_2H_6$ and $TiCl_4 + BCl_3$ systems at P_{tot} = 4 kPa and $m_{B/Ti}$ = 2. The theoretical deposition efficiency for CVD-TiB_2 can be calculated by the aforementioned SOLGASMIX-PV. The theoretical deposition efficiency of the $TiCl_4 + B_2H_6$ system decreases gradually with a decrease in T_{dep}, but that of the $TiCl_4 + BCl_3$ system decreases rapidly below T_{dep} = 1000 K. These trends occurring in the thermodynamic calculations of deposition efficiency may explain the abrupt decrease of deposition rates at T_{dep} below 1000 K for the $TiCl_4 + BCl_3$ system. It may also explain the lower deposition rates in the $TiCl_4 + BCl_3$ system in comparison to the $TiCl_4 + B_2H_6$ system. Fig. 10 illustrates both of these phenomena. Another possible explanation for the abrupt decrease of deposition rate at lower T_{dep} is that BCl_3 gas may be kinetically difficult to react with the $TiCl_4$ vapour at lower T_{dep}.

Table III summarizes the activation energies for the formation of CVD-TiB_2 films reported in the past and that of the CVD-TiB_2 plates obtained in the present work. Besmann and Spear [17] indicated that the activation energy for the formation of CVD-TiB_2 film in the $TiCl_4 + BCl_3$ system was 17 kJ mol^{-1} at T_{dep} = 1473 to 1873 K, and the rate determining process was the diffusion of gaseous species in the boundary layer. They reported that below T_{dep} at 1473 K the activation energy was estimated to be 170 kJ mol^{-1} and the rate determining process was chemical reaction. Randich [22] reported that the activation energy for TiB_2 in the $TiCl_4 + BCl_3$ system was 77 kJ mol^{-1}, but no comment was made on the mechanism of the CVD-TiB_2 formation. Many other investigations [9, 13–15, 18] have reported the influence of T_{dep} on the deposition rates of CVD-TiB_2 in the $TiCl_4 + BCl_3$ system, however, none has mentioned the values of the activation energies or deposition mechanism.

Pierson and Mullendore [18] prepared CVD-TiB_2 films using the $TiCl_4 + B_2H_6$ system at T_{dep} = 873 to 1223 K. The activation energy calculated from T_{dep} dependency was estimated to be 33 kJ mol^{-1}. This value is nearly in agreement with the values (41 to 51 kJ mol^{-1}) obtained in the present work. Fig. 10 shows that the deposition rates reported by Pierson and Mullendore [18] can be extended higher T_{dep} to match those of the present work. The activation energy obtained by the present work (41 to 51 kJ mol^{-1}) is far different from the values reported by Caputo *et al.* [15] and Blandenet *et al.* [13] (about 110 to 190 kJ mol^{-1}).

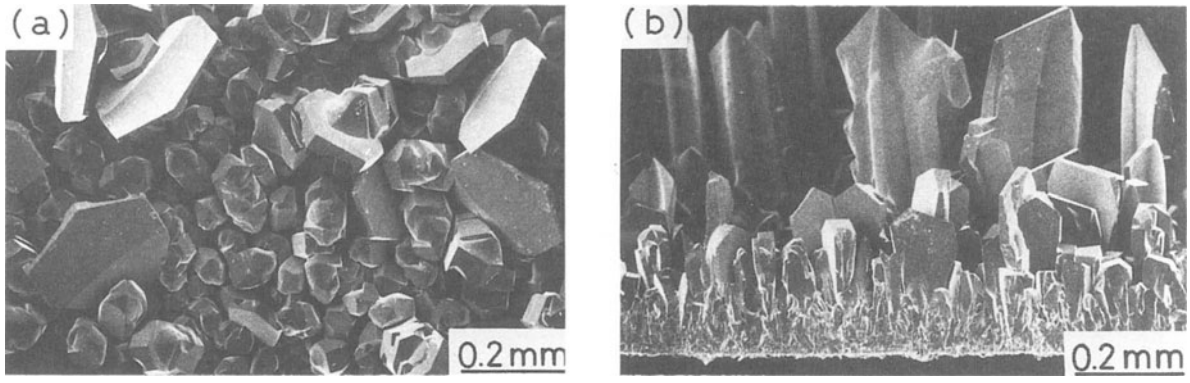

Figure 5 Scanning electron micrographs of the surface (a) and cross-section (b) of columnar CVD-TiB_2 prepared at T_{dep} = 1673 K, P_{tot} = 40 kPa and $m_{B/Ti}$ = 4.

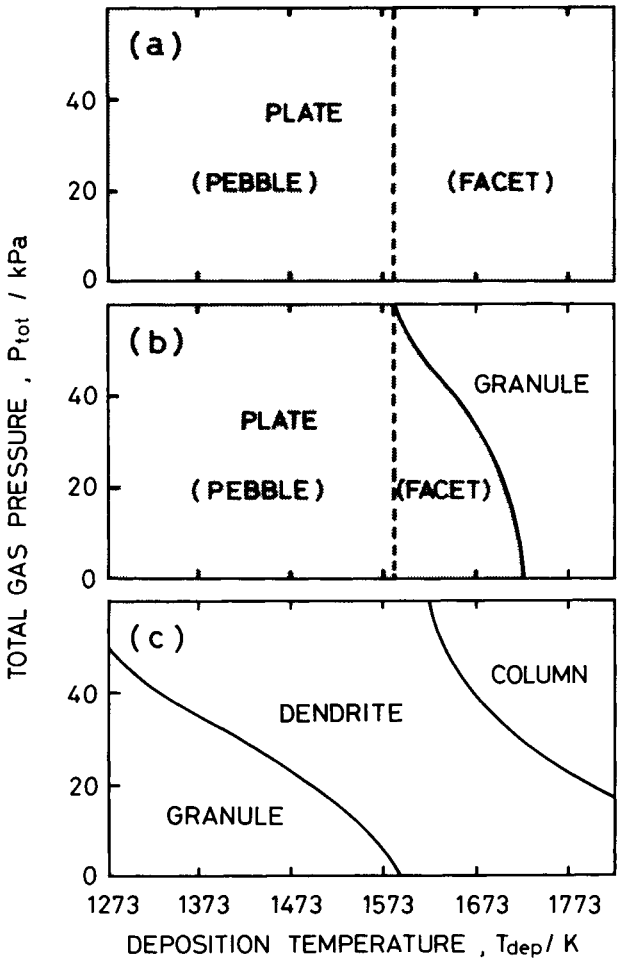

Figure 6 Relationship between CVD conditions and morphology. (a) $m_{B\,Ti} = 0.6$, (b) $m_{B\,Ti} = 2$, (c) $m_{B\,Ti} = 4$.

TABLE III Activation energies for the formation of CVD-TiB_2 plate

System	T_{dep} (K)	E_a (kJ mol^{-1})	Ref.
$TiCl_4 + BCl_3$	1023–1223	188	15
$TiCl_4 + BCl_3$	1273–1473	109	13
$TiCl_4 + BCl_3$	1173–1323	92	9
$TiCl_4 + BCl_3$	1023–1223	53	14
$TiCl_4 + BCl_3$	1473–1873	17	17
$TiCl_4 + B_2H_6$	873–1223	33	18
$TiCl_4 + B_2H_6$	1323–1773	41–51	present work

It can be concluded that the rate determining process for the formation of CVD–TiB_2 in the present work is the diffusion of gaseous species in the boundary layer just as for the case reported by Besmann and Spear [17].

4. Conclusions

The $TiCl_4 + B_2H_6$ system was employed to prepare the CVD–TiB_2 plates at $T_{dep} = 1323$ to 1773 K, $P_{tot} = 4$ to 40 kPa and $m_{B/Ti} = 0.6$ to 4. The following results were obtained.

(1) The high-density and high-purity CVD–TiB_2 plates were obtained at $T_{dep} = 1323$ to 1773 K and $m_{B/Ti} = 0.6$ to 2. The surface structure of the CVD–TiB_2 plates was pebble-like below $T_{dep} = 1573$ K and faceted over $T_{dep} = 1673$ K. When the $m_{B/Ti} = 4$, the morphology of the CVD–TiB_2 changed from granular to dendritic to columnar with increasing T_{dep} and P_{tot}.

(2) The deposition rate of the CVD–TiB_2 plates increased with an increase in T_{dep}. Above $T_{dep} = 1573$ K, the deposition rate increased with an increase

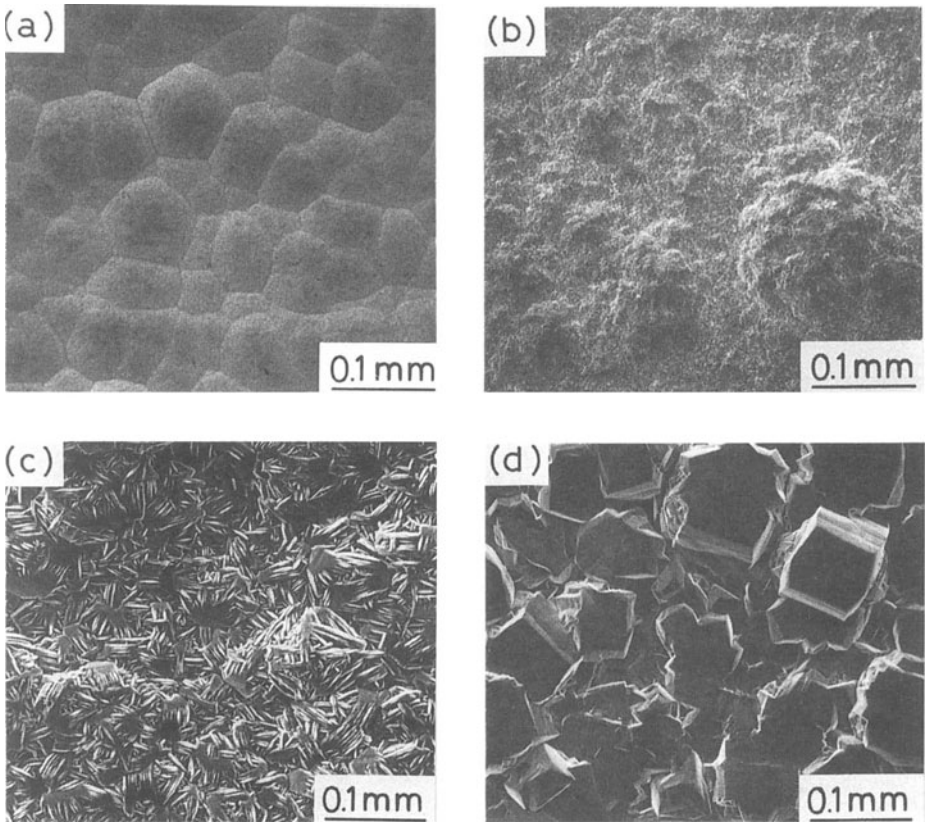

Figure 7 Relationship between deposition temperature (T_{dep}) and the surface structure of CVD–TiB_2 plates prepared at $P_{tot} = 40$ kPa and $m_{B\,Ti} = 0.6$. (a) $T_{dep} = 1473$ K, (b) $T_{dep} = 1573$ K, (c) $T_{dep} = 1673$ K, (d) $T_{dep} = 1773$ K.

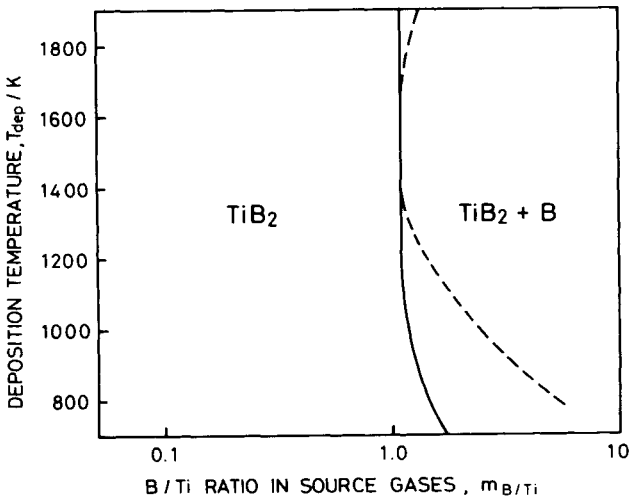

Figure 8 CVD phase diagram based on thermodynamic equilibrium calculations at P_{tot} = 4 kPa. ——: $TiCl_4$ + B_2H_6 system, – – –: $TiCl_4$ + BCl_3 system.

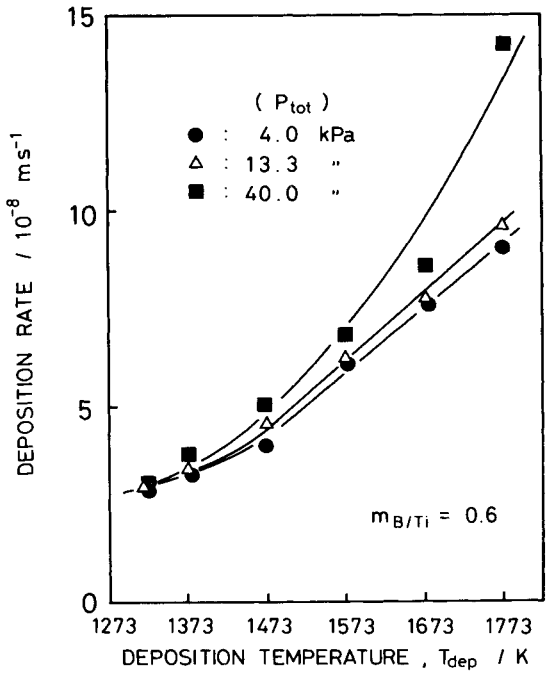

Figure 9 Effect of deposition temperature (T_{dep}) on the deposition rate of CVD–TiB_2 plate.

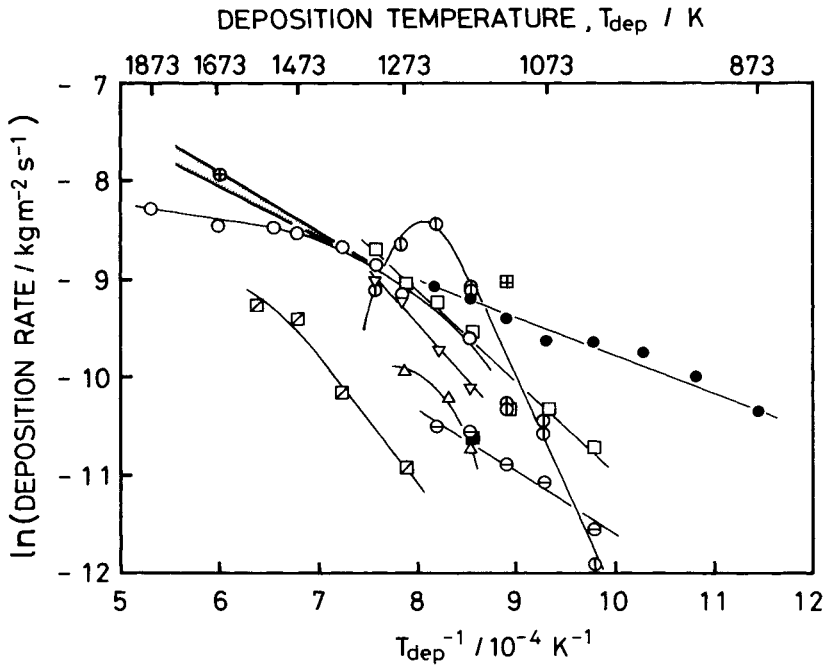

Figure 10 Relationship between deposition rate and deposition temperature (T_{dep}) of CVD–TiB_2 plate. $TiCl_4$ + BCl_3 system ⊕: (8), ▽: (9), ⊞: (12), ⊠: (13), ⊖: (14), ⊕: (15), ○: (17), △: (18), □: (22); $TiCl_4$ + B_2H_6 system ●: (18), ■: (23), ⊡: present work.

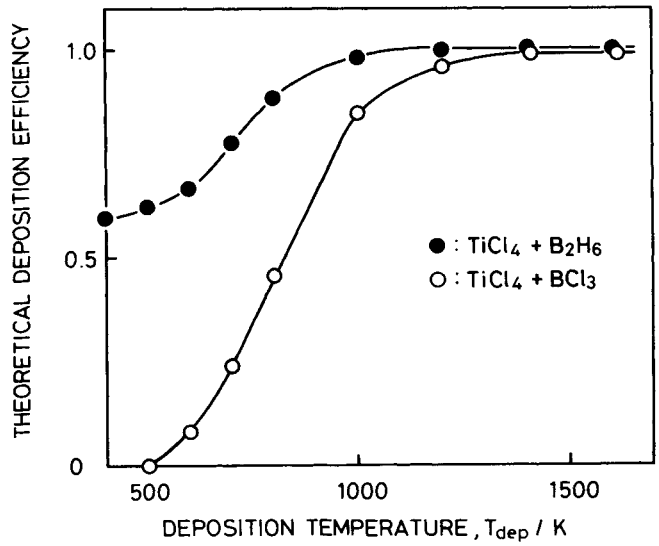

Figure 11 Relationship between theoretical deposition efficiency and deposition temperature (T_{dep}) of CVD–TiB_2. $m_{B/Ti}$ = 2, P_{tot} = 4 kPa.

in P_{tot}. The largest deposition rate of the CVD–TiB_2 plate was 1.4×10^{-7} m sec^{-1} (0.5 mm h^{-1}) at T_{dep} = 1773 K, P_{tot} = 40 kPa and $m_{B/Ti}$ = 0.6. This value (0.5 mm h^{-1}) is the largest among the values reported for either both the $TiCl_4 + BCl_3$ or the $TiCl_4 + B_2H_6$ system.

(3) The activation energies for the formation of the CVD–TiB_2 plates were 41 to 51 kJ mol^{-1}. These values suggest that the rate-determining process is the diffusion of gaseous species in the boundary layer.

Acknowledgment

This research was supported in part by the Grant-in-Aid for Scientific Research under Contract No. 60430019 from the Ministry of Education, Science and Culture, Japan.

References

1. G. AUNER, Y. F. HSIEH and K. R. PADMANABHAN, *Thin Solid Films* **107** (1983) 191.
2. H. O. PIERSON, in "Chemically Vapor Deposited Coatings", edited by H. O. Pierson (American Ceramic Society, Chicago, 1981) p. 27.
3. A. J. BECKER and J. H. BLANKS, *Thin Solid Films* **119** (1984) 241.
4. T. M. BESMANN and K. E. SPEAR, *J. Cryst. Growth* **31** (1985) 60.
5. H. O. PIERSON and D. M. MATTOX, *J. Less-Common Met.* **67** (1979) 381.
6. L. R. SHAPPIRIO and J. J. FINNEGAN, *Thin Solid Films* **107** (1983) 81.
7. R. E. GANNON, R. C. FOLWEILER and T. VASILOS, *J. Amer. Ceram. Soc.* **46** (1963) 496.
8. J. J. GEBHARDT and R. F. CREE, *J. Amer. Ceram. Soc.* **48** (1965) 262.
9. H. O. PIERSON and E. RANDICH, in "Proceedings of the 6th International Conference on Chemical Vapor Deposition, Atlanta, October 1977", edited by L. F. Donaghey, P. Rai-Choudhury and R. N. Tauber (Electrochemical Society, Princeton, 1977) p. 304.
10. K. MOERS, *Z. Anorg. Allg. Chem.* **198** (1931) 243.
11. T. TAKAHASHI and H. KAMIYA, *J. Cryst. Growth* **26** (1974) 203.
12. T. TAKAHASHI and H. ITOH, *J. Cryst. Growth* **49** (1980) 445.
13. G. BLANDENET, Y. LAGARDE, J. P. MORLEVAY and G. UNY, in Proceedings of the 6th International Conference on Chemical Vapor Deposition, Atlanta, October 1977, edited by L. F. Donaghey, P. Rai-Choudhury and R. N. Tauber (Electrochemical Society, Princeton, 1977) p. 330.
14. H. O. PIERSON and A. W. MULLENDORE, *Thin Solid Films* **95** (1982) 99.
15. A. J. CAPUTO, W. J. LACKEY, I. G. WRIGH and P. ANGELINI, *J. Electrochem. Soc.* **132** (1985) 2274.
16. T. M. BESMANN and K. E. SPEAR, *J. Electrochem. Soc.* **124** (1977) 786.
17. *Idem, ibid.* **124** (1977) 790.
18. H. O. PIERSON and A. W. MULLENDORE, *Thin Solid Films* **72** (1980) 511.
19. T. M. BESMANN, ORNL/TM-5775 (April, 1977).
20. "JANAF Thermochemical Tables, 2nd edn, No. NSRDS-NBS-37", edited by D. R. Stull and H. Prophet, U.S. Government Printing Office, Washington, DC (1971).
21. I. BARIN, O. KNACKE, and O. KUBASCHEWSKI, "Thermochemical Properties of Inorganic Substances", Supplement (Springer-Verlag, Berlin, Heidelberg, New York, Verlag Stahleisen m.b.H. Düsseldorf, 1977).
22. E. RANDICH, *Thin Solid Films* **63** (1979) 309.
23. A. W. MULLENDORE, J. B. WHITLEY, H. O. PIERSON and D. M. MATTOX, *J. Vac. Sci. Technol.* **18** (1981) 1049.

Received 15 November 1988
and accepted 26 April 1989